CMS Conference Report

31 May 2006

Search for the Light Charged Higgs in CMS

M. Hashemi[1)a)],

CMS collaboration

Abstract

In this report the CMS potential for the light charged Higgs boson discovery in the Minimal Supersymmetric Standard Model is presented. First the latest results of the Tevatron and LEP experiments on the light charged Higgs search are reminded. In the rest of the report the perspectives of CMS for the light charged Higgs search are presented with description of some details of the analysis. The results are based on the full simulation and reconstruction of the CMS detector including the systematic uncertainties on the background determination. Finally the 5σ discovery contour for an integrated luminosity of $30\mathrm{fb}^{-1}$ is shown.

Presented at *IPM School and Conference on Lepton and Hadron Physics*,
Tehran, Iran, May 15-20, 2006

[1)] IPM, Tehran, Iran

[a)] also at Sharif University of Technology

1 Introduction

The Minimal Supersymmetric extension to the Standard Model (MSSM) [1] requires the introduction of two Higgs doublets in order to preserve the supersymmetry. Five physical Higgs particles are predicted, two CP-even (h,H), one CP-odd (A) and two charged ones ($H^{\pm}$). All couplings and masses of the MSSM Higgs sector are determined at the lowest order by two independent parameters, which are generally chosen as $\tan\beta = v_2/v_1$, the ratio of the vacuum expectation values of the two Higgs doublets, and the pseudo–scalar Higgs boson mass m_A. Since the charged Higgs boson is a crucial signature of the MSSM, it is presently considered as one of the most interesting particles in the MSSM Higgs sector.

The latest results from the LEP Higgs working group concerning the indirect search for neutral MSSM Higgs bosons provide a lower mass limit of 125 GeV/c^2 for $m_{H^{\pm}}$ at $\tan\beta > 10$ [2]. Results from direct searches at LEP give instead a lower limit on the charged Higgs boson mass of $\sim$ 90 GeV/c^2 for $BR(H^+ \to \tau\nu) \simeq 1$ [3]. Figure 1 shows the excluded region obtained in 2006 by the LEP Higgs working group. Direct and indirect searches

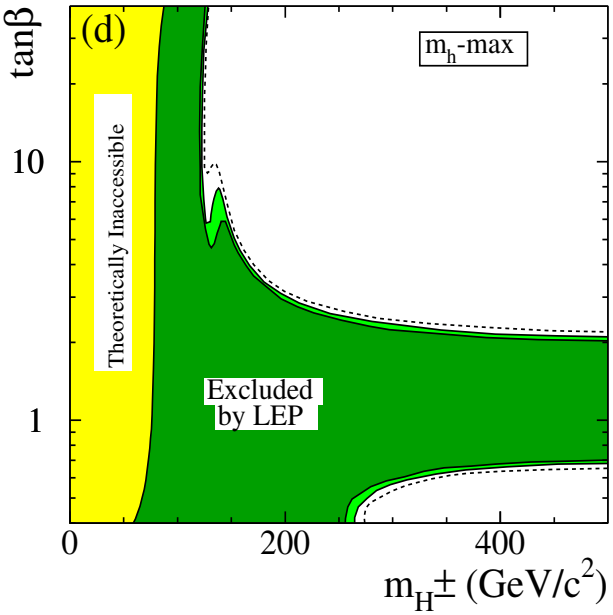

Figure 1: The excluded region at 99.7% C.L. (Dark Green) obtained by the LEP Higgs working group.

performed at the Tevatron lead to some exclusion region in the parameter space for $\tan\beta > 50$ and $\tan\beta < 1$ [4, 5]. Figure 2 shows the excluded region obtained by Tevatron in the D0 and CDF experiments. In the study presented in this report the light charged Higgs ($m_{H^{\pm}} < m_t - m_b$) is searched for in the channel $H^{\pm}_{MSSM} \to \tau^+\nu_\tau$, $\tau \to$hadrons in the mass range $125 < m_{H^{\pm}} < 170$ GeV/c^2 [6]. The mass range chosen is the most critical since for Higgs boson masses close to the top mass the signal rate is low. Proving that the discovery is attainable in this mass range would imply that the light charged Higgs boson can be discovered also at lower masses. All results are obtained according to the LEP $m_{h^0} - \max$ benchmark scenario [2] with the following choice of the MSSM parameters: SU(2) gaugino mass $M_2 = 200$ GeV/c^2, $\mu = +200$ GeV/c^2, gluino mass $M_{\tilde{g}} = 800$ GeV/c^2, SUSY breaking mass parameter $M_{SUSY} = 1$ TeV/c^2 and stop mixing parameter $X_t = \sqrt{6}\, M_{SUSY}$ ($X_t = A_t + \mu cot\beta$). The $m_{h^0} - \max$ scenario is one of the LEP benchmark scenarios designed to maximize the upper limit on m_{h^0} by non-zero stop mixing parameter thus providing a wider available parameter space compared to the case of $no - mixing$ scenario in which the stop mixing parameter is set to zero and the available parameter space is smaller. The top quark mass is set to 175 GeV/c^2.

2 Signal and background simulation, cross sections and branching ratios

The MSSM charged Higgs boson can be produced in top quark decays, $t \to H^+b$, if $m_{H^{\pm}} < m_t - m_b$. In this report the case of $W^{\pm}$ leptonic decay (e or μ) is described. The background channels consist of $t\bar{t}$ events with at least a single lepton (e or μ) and τ-jets or jets which could fake τ-jets, $W^{\pm} + 3$ jets events and also single top events which have, however, a small contribution. A total NLO $t\bar{t}$ cross section of 850 pb is used in this report [8] for calculating the cross sections of the different final states. The cross section of $W^{\pm} + 3$ jets events is obtained with the MadEvent generator [9] with some preselection cuts: $E_T^{jet} > 20$ GeV, $|\eta| < 2.5$ for all final state jets and

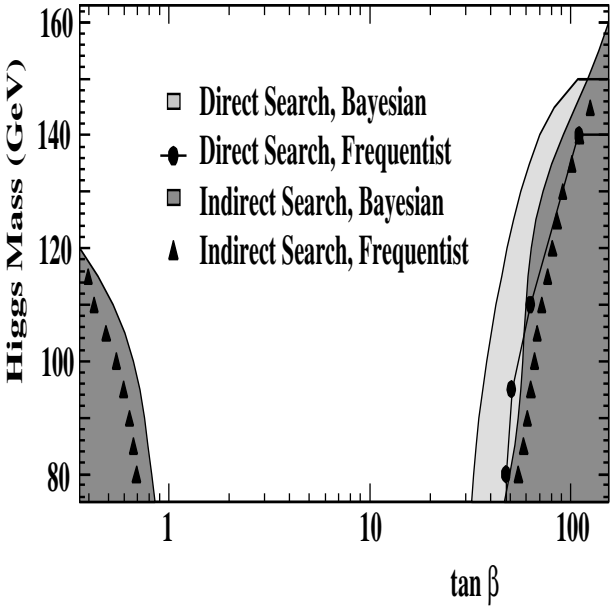

Figure 2: The excluded region at 95% C.L. obtained by D0 and CDF at Tevatron.

$R = \sqrt{(\Delta\eta)^2 + (\Delta\phi)^2} = 0.5$ for all pairs of final state jets. The branching ratio of top decay to charged Higgs depends on both $m_{\mathrm{H}^\pm}$ and $\tan\beta$ as shown in Fig. 3a. The corresponding top decay to $\mathrm{W}^\pm\mathrm{b}$ (Fig. 3b) decreases with increasing $\tan\beta$ while keeping the sum of the branching ratios around one (for $m_{\mathrm{H}^+} \simeq 170$ GeV/c^2 the $\mathrm{t} \to \mathrm{W}^+\mathrm{s}$ branching ratio is of the same order as that of $\mathrm{t} \to \mathrm{H}^+\mathrm{b}$ therefore these two plots are not similar for $m_{\mathrm{H}^+} = 170$ GeV/c^2). Figure 4 shows the $\mathrm{H}^\pm$ decay branching ratio in different final states for $\tan\beta = 20$.

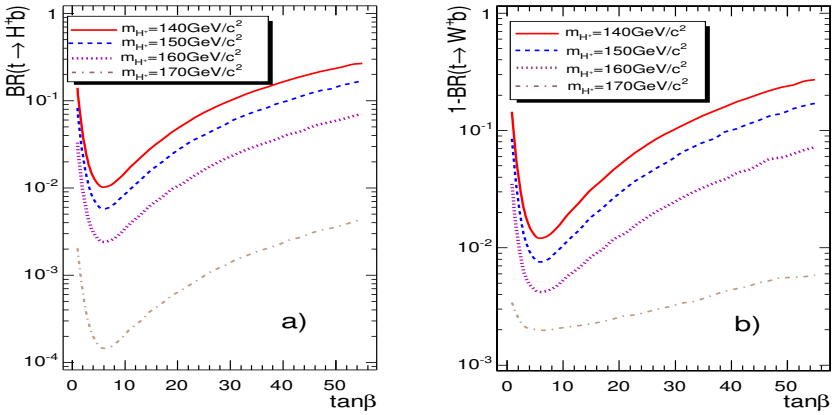

Figure 3: a)Branching ratio of top decay to $\mathrm{H}^\pm$ vs $\tan\beta$, b)Branching ratio of top decay to $\mathrm{W}^\pm$ vs $\tan\beta$

Table 1: Cross section times branching ratio of $\mathrm{t\bar{t}} \to \mathrm{H}^\pm\mathrm{W}^\mp\mathrm{b\bar{b}} \to \tau\nu_\tau\ell\nu_\ell\mathrm{b\bar{b}}, \tau \to$ hadrons for $\tan\beta = 20$

$m_{\mathrm{H}^\pm}$ (GeV/c^2)	140	150	160	170
Cross section [pb]	10.70	5.06	1.83	0.157

Table 2: Cross section times branching ratio of $\mathrm{t\bar{t}} \to \mathrm{H}^+\mathrm{H}^-\mathrm{b\bar{b}} \to \tau^+\nu_\tau\tau^-\bar{\nu}_\tau\mathrm{b\bar{b}}, \tau^\pm \to$ hadrons (leptons) for $\tan\beta = 20$

$m_{\mathrm{H}^\pm}$ (GeV/c^2)	140	150	160
Cross section (pb)	0.91	0.19	0.02

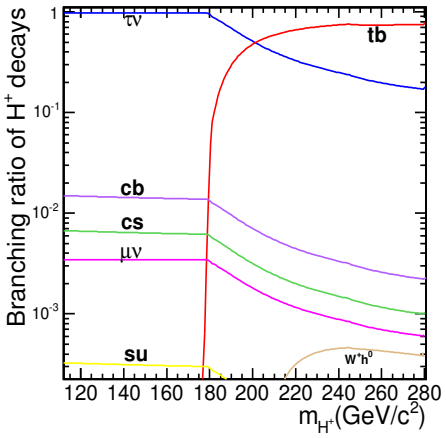

Figure 4: Branching ratio of $\mathrm{H}^{\pm}$ decays for different $m_{\mathrm{H}^{\pm}}$ at $\tan\beta = 20$

Table 1 shows the cross section times branching ratio of $\mathrm{t\bar{t}} \to \mathrm{H}^{\pm}\mathrm{W}^{\mp}\mathrm{b\bar{b}}$ events for $\tan\beta = 20$. Due to the small cross section of $\mathrm{t\bar{t}} \to \mathrm{H}^{+}\mathrm{H}^{-}\mathrm{b\bar{b}}$ as shown in Table 2 only $\mathrm{t\bar{t}} \to \mathrm{H}^{\pm}\mathrm{W}^{\mp}\mathrm{b\bar{b}}$ events were generated and simulated as signal events for $m_{\mathrm{H}^{\pm}} < 170$ GeV/c^2. For $m_{\mathrm{H}^{\pm}} = 170$ GeV/c^2 both $\mathrm{t\bar{t}}$ + gb and $\mathrm{gg} \to \mathrm{t\bar{b}H}^{\pm}$ are used for comparison. The NLO cross section times branching ratio of signal events with $m_{\mathrm{H}^{+}} \simeq m_{\mathrm{t}}$ is listed in Table 3. Finally the cross section of the main background channels are shown in Table 4.

Table 3: Cross section times branching ratio of signal events for $m_{\mathrm{H}^{\pm}} \simeq m_{\mathrm{t}}$ according to NLO calculations in [7] for $\tan\beta = 20$.

Channel	$\mathrm{gb} \to \mathrm{tH}^{\pm} \to \ell\nu_{\ell}\mathrm{b}\tau\nu_{\tau}$ ($\tau \to$ hadrons) $m_{\mathrm{H}^{\pm}} = 170$ GeV/c^2	$\mathrm{gg} \to \mathrm{tbH}^{\pm} \to \ell\nu_{\ell}\mathrm{bb}\tau\nu_{\tau}$ ($\tau \to$ hadrons) $m_{\mathrm{H}^{\pm}} = 170$ GeV/c^2
Cross section [pb]	0.14	0.297

Table 4: Cross section times branching ratio of background events

Channel	$\mathrm{t\bar{t}} \to \mathrm{W}^{+}\mathrm{W}^{-}\mathrm{bb}$ $\to \ell\nu_{\ell}\tau\nu_{\tau}\mathrm{b\bar{b}}$ ($\tau \to$ hadrons)	$\mathrm{t\bar{t}} \to \mathrm{W}^{+}\mathrm{W}^{-}\mathrm{bb}$ $\to \ell\nu_{\ell}\ell'\nu_{\ell'}\mathrm{b\bar{b}}$ $\ell, \ell' =$ e or μ	$\mathrm{t\bar{t}} \to \mathrm{W}^{+}\mathrm{W}^{-}\mathrm{b\bar{b}}$ $\to \ell\nu_{\ell}\mathrm{jjb\bar{b}}$	$\mathrm{W}^{\pm} + 3$ jets $\mathrm{W}^{\pm} \to$ e or μ
Cross section [pb]	25.8	39.7	245.6	840

3 Event selection

Full simulation of the detector response was achieved with CMSIM [10] or OSCAR [11] including pile–up events corresponding to a luminosity of $2 \times 10^{33}\mathrm{cm}^{-2}\mathrm{s}^{-1}$. The full reconstruction of the detector response and event analysis was performed with the ORCA package [12]. The event selection is as the following:

- Event trigger
  Events are triggered if there is a muon with $p_T > 14$ GeV, $|\eta| < 2.1$ or an electron with $p_T > 29$GeV, $|\eta| < 2.4$. At HLT harder cuts are applied such as $p_T > 19$ GeV and isolation requirements for muons [13].
- Jet reconstruction, selection and b-tagging
  Jets were reconstructed with the Iterative Cone algorithm [13] with a cone size $R = \sqrt{(\Delta\eta)^2 + (\Delta\phi)^2} = 0.5$. Jets were selected within $|\eta| < 2.4$ and requiring $E_T^{\mathrm{jet}} > 40$ GeV. There should be at least three jets in the event to be accepted.
  The b-tagging is done by Impact Parameter Significance method and one b-jet is required in the event with kinematic cuts the same as those applied on jets.

- Offline τ tagging
  The τ reconstruction and selection is performed offline starting from the Level 1 τ-like energy deposits in the calorimeters ([13]). A regional jet reconstruction is performed around the direction of the Level 1 τ objects; the raw jet tranverse energy is required to be $E_T^{\rm jet} > 20$ GeV. The contribution from electrons faking τ-jets can be reduced by requiring the hottest HCAL tower $\rm E_T$ to be larger than 2 GeV (only towers belonging to jets are considered). In the next step a matching cone with $\Delta \rm R = 0.1$ is defined around the jet axis. Tracks with $p_T > 1$ GeV/c are searched for within the matching cone and the largest p_T track is identified and a signal cone with $\Delta \rm R = 0.07$ is defined around its direction. The signal vertex is considered as the vertex from which the leading track originates. Then an isolation cone with $\Delta \rm R = 0.4$ is defined around the leading track to check the tracker isolation requirement. If no track from the signal vertex is found with $p_T > 1$ GeV/c in the isolation cone except for those falling in the signal cone, the isolation is satisfactory. The electromagnetic isolation parameter (Eq. 1) is used to suppress the contamination arising from quark and gluon jets [14]:

$$P_{\rm isol.} = \sum_{\rm crystals, \Delta R_{crystal,\tau-jet}<0.4} E_{T\,\rm crystal} - \sum_{\rm crystals, \Delta R_{crystal,\tau-jet}<0.13} E_{T\,\rm crystal} < 5.6\ \rm GeV \qquad (1)$$

  When a jet satisfies all requirements mentioned above, it is identified as a τ-jet candidate. A cut on the transverse energy of the τ jet, $E_{T\tau} > 40$ GeV, can be applied to suppress the background. Since the leading track in the jst is more energetic in signal events than in background events, a cut on the τ energy carried by the leading track in the signal cone is applied by requiring $p_{\rm leading\ track}/E_\tau > 0.8$. The total charge of all tracks contained in the signal cone of an identified τ-jet gives an estimate of the τ-lepton charge. The sum of the charges of the event trigger lepton (e orμ) and of the τ-lepton is hence required to be $Q(\ell) + Q(\tau) = 0$, since they originate from mother particles of opposite charges ($\rm H^\pm, W^\mp$).

- Missing E_T reconstruction
  The missing transverse energy reconstruction is performed by summing all the Ecal energy deposits plus the Hcal towers and correcting for muons (if any in the event). The raw energy jets of jets involved in the $E_T^{\rm miss}$ reconstruction are corrected [15] to improve their energy resolution. Only jets with raw jet $E_T > 30$ GeV are used; this cut is optimized to improve the $E_T^{\rm miss}$ resolution. A cut at $E_T^{\rm miss} > 70$ GeV is applied to increase the signal to background ratio.

4 Signal and background selection efficiencies

The summary of all event selection requirements together with the corresponding efficiencies is given in Tables 5, 6 (signal) and Table 7 (background). As mentioned in Section 2 the number of signal events from $\rm t\bar{t}$ and gb fusion for $m_{\rm H^\pm} = 170$ GeV/c^2 should actually be added together and then compared to gg fusion process. No significant difference is seen between $\rm t\bar{t}$+gb and gg. The one b-jet requirement mentioned in Section 3.2 is decomposed into two different steps: firstly events with at least one b-jet are accepted, secondly events with more than one b-jet are rejected. The first requirement has a higher selection efficiency for background events, however, the second cut rejects background events reasonably (more than $\sim 30\%$) at the expense of losing $\sim 5 - 20\%$ of signal events. The efficiency of the second cut for signal events increases with larger $m_{H^\pm}$, i.e. with lower signal cross section. Hence there is little loss where the signal rate is low.

Results can be extrapolated to other $\tan\beta$ values by using the branching ratios of Figs. 3a, 3b and 4. The effect of a larger $\tan\beta$ appears only as some increase in the signal rate and no kinematic effect is expected. Selection efficiencies are then expected to be independent from $\tan\beta$. Different $\tan\beta$ values were investigated in this study for different masses of charged Higgs. In the next sections the results are presented and the final conclusions are drawn.

5 Contribution of other signal and background final states

Contribution of other signal final states is estimated to be an additional factor of $\sim 2\%$ to the number of signal events [6]. The single top background produces about 60 events after all selection cuts and is taken into account in all calculations. The contribution of other background events such as $\rm W^\pm bb$ with $\rm W^\pm \to e\nu_e$ or $\mu\nu_\mu$ and Zbb followed by the decay $\rm Z \to ee$ or $\tau\tau$ are also estimated to be negligible.

Table 5: List of selection cuts and their efficiencies for signal events with $m_{\mathrm{H}^\pm} < 170$ GeV/c^2 for $\tan\beta = 20$. Numbers in each row show the remaining cross section after applying the corresponding cut. Numbers in parentheses are relative efficiencies in percent.

	$\mathrm{t\bar{t}} \to \mathrm{H}^\pm\mathrm{W}^\mp\mathrm{bb}$ $\to \ell\nu_\ell\tau\nu_\tau\mathrm{b\bar{b}}$ $m_{\mathrm{H}^\pm} = 140$ GeV/c^2	$\mathrm{t\bar{t}} \to \mathrm{H}^\pm\mathrm{W}^\mp\mathrm{bb}$ $\to \ell\nu_\ell\tau\nu_\tau\mathrm{b\bar{b}}$ $m_{\mathrm{H}^\pm} = 150$ GeV/c^2	$\mathrm{t\bar{t}} \to \mathrm{H}^\pm\mathrm{W}^\mp\mathrm{bb}$ $\to \ell\nu_\ell\tau\nu_\tau\mathrm{b\bar{b}}$ $m_{\mathrm{H}^\pm} = 160$ GeV/c^2
$\sigma \times$ BR[fb]	10.7×10^3	5060.	1830.
L1 + HLT	5170.5(48.3)	2456.3(48.5)	888.9(48.6)
>= 3 jets	1889.7(36.5)	795.0(32.4)	264.3(29.7)
≥ 1 b jet	1103.5(58.4)	427.4(53.8)	131.4(49.7)
< 2 b jets	883.0(80.0)	358.7(83.9)	119.2(90.7)
Having L1 τ	878.4(99.5)	357.4(99.6)	119.0(99.8)
τ-jet reconstruction	875.0(99.6)	356.5(99.7)	118.8(99.8)
Hottest HCAL tower $E_T > 2$ GeV	778.0(88.9)	316.1(88.6)	105.9(89.1)
Tracker isolation	378.2(48.6)	163.5(51.7)	52.7(49.8)
Ecal isolation	292.9(77.4)	134.2(82.1)	43.1(81.8)
τ $E_T > 40$ GeV	244.3(83.4)	113.0(84.2)	36.5(84.7)
$p_{\text{leading track}}/E_\tau > 0.8$	102.3(41.9)	50.7(44.8)	16.8(45.9)
$Q(\ell) + Q(\tau) = 0$	88.0(86.0)	42.4(83.6)	14.6(87.0)
$E_T^{\text{miss}} > 70$ GeV	51.0(58.0)	25.4(59.9)	9.2(63.3)
Expected Number of events after 10 fb^{-1}	510	254	92

6 Results with systematic uncertainties

Since the number of background events after all selection cuts is large enough (more than 1000 events), the significance can be defined as

$$S = \frac{N_{\text{obs.}}^{\text{MSSM}} - (N_{\text{W+3 jets}}^{\text{SM}} + N_{\mathrm{t\bar{t}}}^{\text{SM}})}{\sqrt{N_{\text{W+3 jets}}^{\text{SM}} + N_{\mathrm{t\bar{t}}}^{\text{SM}} + (\Delta N_{\text{W+3 jets}}^{\text{SM}})^2 + (\Delta N_{\mathrm{t\bar{t}}}^{\text{SM}})^2}} \tag{2}$$

The approach for including systematic uncertainties in the signal statistical significance calculation have been described in detail in [6]. Therefore here only the sources of uncertainties and how they are taken into account are presented.
The total systematic undertainty on the $\mathrm{t\bar{t}}$ background can be expressed as

$$\Delta_{\text{sys.}}^{\mathrm{t\bar{t}}} = \Delta_{\text{lepton reconstruction}} \oplus \Delta_{\geq 3 \text{ jet selection}} \oplus \Delta_{1\ \mathrm{b-jet\ tagging}} \oplus \Delta_{1\ \tau\ \text{tagging}} \oplus \Delta_{\text{lumi.}} \oplus \Delta_{\text{theo.}}^{\mathrm{t\bar{t}}} \tag{3}$$

The $\mathrm{W}^\pm + 3$ jets background uncertainty is estimated as the following

$$\Delta_{\text{sys.}}^{\mathrm{W}^\pm+3\text{ jets}} = \Delta_{\text{stat.}} \oplus \frac{\Delta N_B^{\mathrm{t\bar{t}}}}{N_B^{\mathrm{W}^\pm+3\text{ jets}}} \oplus \Delta_{3\ \mathrm{non-b-jet}} \oplus \Delta_{\mathrm{b-jet\ mistagging}} \oplus \Delta_{\tau\ \text{mistagging}} \tag{4}$$

In Eq. 4, $\Delta N_B^{\mathrm{t\bar{t}}}$ is the uncertainty of the number of $\mathrm{t\bar{t}}$ events in the background area and $N_B^{\mathrm{W}^\pm+3\text{ jets}}$ is the number of $\mathrm{W}^\pm + 3$ jets events in the background area.
Table 8 shows the values of individual uncertainties which were used in the signal significance calculation for 30 fb^{-1}. These are the minimum values of uncertainties in the duration of an integrated luminosity of 30 fb^{-1} which would be reached at the end of this period.

6.1 Final result and the 5σ discovery contour with systematic uncertainties

Equation 2 is used to calculate the signal statistical significance at 30fb^{-1} for different $\tan\beta$ values. Table 9 shows the signal significance for different $\mathrm{m_{H^+}}$ and $\tan\beta$ values at 30 fb^{-1}. The extrapolation to large $\tan\beta$ values shows that a 5σ significance for $m_{\mathrm{H}^+} = 170$ GeV/c^2 is obtained only for $\tan\beta \geq 100$.

The results listed in Table 9 are shown in the form of a 5σ discovery contour in Fig. 5. The result of introducing the systematic uncertainties in calculation of the signal significance reduces the observability of $m_{\mathrm{H}^\pm}$ for $\tan\beta < 50$.

Table 6: List of selection cuts and their efficiencies for signal events with $m_{\mathrm{H}^{\pm}} = 170$ GeV/c^2 for $\tan\beta = 20$. Numbers in each row show the remaining cross section after applying the corresponding cut. Numbers in parentheses are relative efficiencies in percent.

	$\mathrm{t\bar{t}} \to \mathrm{H}^{\pm}\mathrm{W}^{\mp}\mathrm{bb}$ $\to \ell\nu_{\ell}\tau\nu_{\tau}\mathrm{b\bar{b}}$ $m_{\mathrm{H}^{\pm}} = 170$ GeV/c^2	$\mathrm{gb} \to \mathrm{tH}^{\pm}$ $\to \ell\nu_{\ell}\tau\nu_{\tau}\mathrm{b}$ $m_{\mathrm{H}^{\pm}} = 170$ GeV/c^2	$\mathrm{gg} \to \mathrm{tb\bar{H}}^{\pm}$ $\to \ell\nu_{\ell}\tau\nu_{\tau}\mathrm{b\bar{b}}$ $m_{\mathrm{H}^{\pm}} = 170$ GeV/c^2
$\sigma \times$ BR[fb]	157.	140.	297.
L1 + HLT	78.0(49.7)	70.5(50.4)	145.4(48.9)
>= 3 jets	23.2(29.7)	21.7(30.7)	55.3(38.0)
$\geq$ 1 b jet	11.5(49.4)	11.7(54.1)	31.9(57.7)
$<$ 2 b jets	10.9(94.8)	10.0(85.5)	25.8(80.9)
Having L1 τ	10.8(99.8)	10.0(99.6)	25.7(99.4)
τ-jet reconstruction	10.8(99.9)	10.0(99.9)	25.5(99.1)
Hottest HCAL tower $E_T > 2$GeV	9.6(88.4)	8.9(88.8)	22.6(88.9)
Tracker isolation	4.9(51.3)	5.1(57.2)	11.4(50.5)
Ecal isolation	4.2(84.9)	4.3(84.5)	9.6(84.4)
τ $E_T > 40$GeV	3.8(90.9)	3.9(90.6)	8.6(89.2)
$p_{\text{leading track}}/E_{\tau} > 0.8$	1.6(41.7)	1.8(45.9)	3.4(39.6)
$Q(\ell) + Q(\tau) = 0$	1.3(84.4)	1.6(87.2)	2.8(82.6)
$E_T^{\text{miss}} > 70$ GeV	0.8(61.7)	1.0(65.2)	1.6(55.3)
Expected Number of events after 10 fb^{-1}	8	10	16

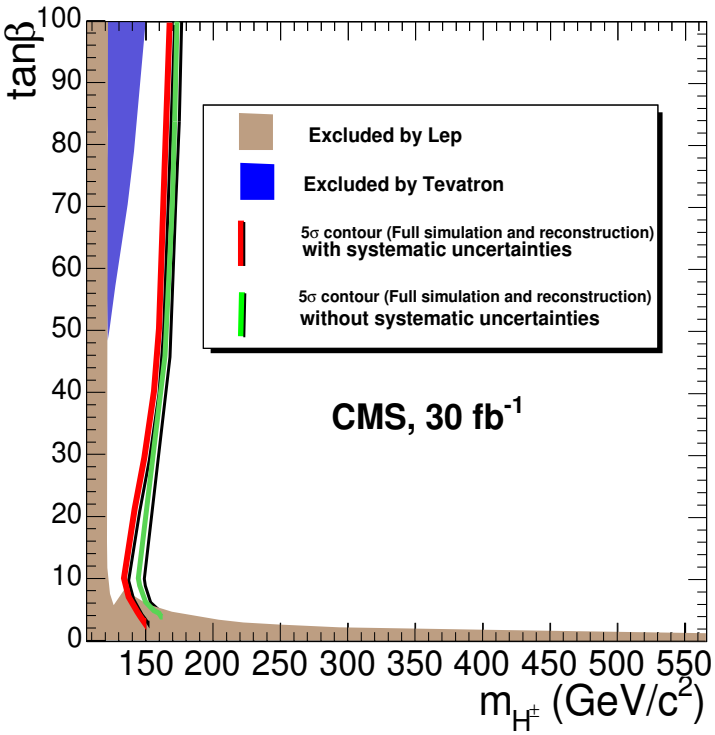

Figure 5: The 5σ contour in $(m_{\mathrm{H}^{+}}, \tan\beta)$ plane for the light charged Higgs discovery including the effect of systematic uncertainties.

For $\tan\beta > 50$ the signal cross section increases and the effect of the uncertainties becomes small. The light charged Higgs discovery potential of CMS was presented in the $\mathrm{t\bar{t}} \to \mathrm{H}^{\pm}\mathrm{W}^{\mp}\mathrm{b\bar{b}} \to \ell\nu_{\ell}\tau\nu_{\tau}\mathrm{b\bar{b}}$ ($\tau \to$hadrons) channel. Results correspond to an integrated luminosity of 30 fb^{-1} including low uminosity pile–up events. The systematic uncertainties are evaluated and included. It was shown that the effect of the systematic uncertainties is

Table 7: List of selection cuts and their efficiencies for background events. Numbers in each row show the remaining cross section after applying the corresponding cut. N umbers in parentheses are relative efficiencies in percent.

	$t\bar{t} \to W^+W^-b\bar{b}$ $\to \ell\nu_\ell\tau\nu_\tau b\bar{b}$	$t\bar{t} \to W^+W^-b\bar{b}$ $\to \ell\nu_\ell\ell'\nu_{\ell'}b\bar{b}$	$t\bar{t} \to W^+W^-b\bar{b}$ $\to \ell\nu_\ell jjb\bar{b}$	$W^\pm + 3$ jets $W^\pm \to \ell\nu_\ell$
$\sigma \times$ BR[fb]	25.8 $\times 10^3$	39.8 $\times 10^3$	245.6$\times 10^3$	840.$\times 10^3$
L1 + HLT	12101.2(46.9)	28429.1(71.4)	99506.6(40.5)	287280(34.2)
>= 3 jets	5105.2(42.2)	11306.6(39.8)	66038.6(66.4)	114050(39.7)
≥ 1 b jet	3428.3(67.1)	7622.0(67.4)	43433.0(65.8)	24292.7(21.3)
< 2 b jets	2325.7(67.8)	5262.7(69.0)	29003.4(66.8)	21207.5(87.3)
Having L1 τ	2310.7(99.3)	5233.7(99.4)	28698.8(98.9)	20613.7(97.2)
τ-jet reconstruction	2303.6(99.7)	5224.4(99.8)	28465.0(99.2)	19438.7(94.3)
Hottest HCAL tower $E_T > 2$GeV	2034.1(88.3)	3850.6(73.7)	26635.1(93.6)	17125.5(88.1)
Tracker isolation	798.7(39.3)	1120.6(29.1)	6653.3(25.0)	5411.7(31.6)
Ecal isolation	545.6(68.3)	519.5(46.3)	2952.8(44.4)	2554.3(47.2)
τ $E_T > 40$GeV	405.8(74.4)	341.8(65.8)	1946.8(65.9)	1312.9(51.4)
$p_{\text{leading track}}/E_\tau > 0.8$	123.5(30.4)	131.9(38.6)	377.9(19.4)	224.5(17.1)
$Q(\ell) + Q(\tau) = 0$	95.7(77.5)	56.7(43.0)	78.8(20.9)	27.1(12.1)
$E_T^{\text{miss}} > 70$ GeV	51.6(53.9)	29.3(51.8)	36.6(46.4)	10.7(39.3)
Expected Number of events after 10 fb^{-1}	516	293	366	107

Table 8: The values of different experimental and theoretical uncertainties used for $t\bar{t}$ and $W^\pm + 3$ jets background events at 30 fb^{-1}.

Scale uncertainty of $t\bar{t}$ cross section	5%
PDF uncertainty of $t\bar{t}$ cross section	2.5%
b-tagging	5%
τ-tagging	4%
Lepton identification	2%
Jet energy scale	3%
Mistagging a non-b-jet as a b-jet	5%
Mistagging a jet as a τ-jet	2%
Non-b-jet identification (anti-b-tagging)	5%
Luminosity uncertainty	5%

a decrease of 5-10 GeV/c^2 the observable charged Higgs mass for $\tan\beta < 50$. Since for $m_{H^\pm} > 160$ GeV/c^2 the signal rate becomes small the 5σ discovery contour shows a small growth for $m_{H^\pm} \geq 160$ GeV/c^2 and the charged Higgs mass of 170 GeV/c^2 is observable at $\tan\beta \simeq 100$.

7 Acknowledgement

I would like to thank Ritva Kinnunen for initiating the idea of this analysis with her original work and for the nice discussions. I would like to thank A. Nikitenko who played the main role in conducting this analysis and also Prof. Arfaei and M. Baarmand for their supervision. Many thanks to R. Tenchini for reading the manuscript of this report and useful comments.

References

[1] S.P. Martin, A Supersymmetry Primer, hep-ph/9709356

[2] ALEPH, DELPHI, L3 and OPAL Collaborations, The LEP Working Group for Higgs Boson Searches, CERN-PH-EP/2006-001, hep-ex/0602042

[3] ALEPH, DELPHI, L3 and OPAL Collaborations, The LEP Working Group for Higgs Boson Searches, LHWG note 2001-05

Table 9: The signal significance for different $m_{(\mathrm{H}^+)}$ and $\tan\beta$ values at 30 fb^{-1} including systematic uncertainties.

	$\tan\beta = 10$	$\tan\beta = 20$	$\tan\beta = 30$	$\tan\beta = 40$	$\tan\beta = 50$
$m_{\mathrm{H}^+} = 140$ GeV/c^2	1.60	5.02	9.43	15.00	20.17
$m_{\mathrm{H}^+} = 150$ GeV/c^2	0.96	2.50	4.70	8.61	12.71
$m_{\mathrm{H}^+} = 160$ GeV/c^2	0.33	0.93	1.66	3.76	5.98
$m_{\mathrm{H}^+} = 170$ GeV/c^2	0.07	0.21	0.46	0.75	1.19

[4] V.M. Abazov et al., hep-ex/0102039

[5] B. Abbott et al., Phys. Rev. Lett **82**(4975)1999

[6] M. Baarmand, M. Hashemi, A. Nikitenko, **CMS NOTE 2006-056**

[7] E.L. Berger et al., hep-ph/0312286, `http://pheno.physics.wisc.edu/~plehn/charged_higgs/`

[8] M.L. Mangano et al., CERN Yellow Report, ID: 2000-004, Workshop on Standard Model Physics (and more) at the LHC, hep-ph/0003033

[9] `http://madgraph.hep.uiuc.edu`

[10] `http://www-collider.physics.ucla.edu/cms/cmsim/`

[11] `http://cmsdoc.cern.ch/oscar/`

[12] `http://cmsdoc.cern.ch/orca/`

[13] The Trigger and Data Acquisition Project, Volume II, Technical Design Report, CERN/LHCC 2002-26, CMS TDR 6.2

[14] A. Nikitenko et al., **CMS NOTE 2000-055**

[15] A. Nikitenko et al., **CMS NOTE 2001-040**